Stereoscopic PIV measurements of the flow past a circular cylinder at Reynolds number 15000

Parker, K.[1], von Ellenrieder, K. D[2] and Soria, J[1]

[1]Laboratory for Turbulence Research in Aerospace & Combustion
Mechanical Engineering, Monash University
Clayton Campus, Victoria, 3800 AUSTRALIA
[2]Dept. Ocean Engineering
Florida Atlantic University
Dania Beach, FL 33004-3023, USA

Abstract

Stereoscopic PIV measurements are conducted on a 2D stationary circular cylinder at Reynolds number 15000, based on cylinder diameter. The experiments form part of the validation of an in-house developed stereoscopic PIV reconstruction procedure. The purpose of this paper is to discuss the difficulties associated with stereo PIV measurements in liquid flows in the context of high Reynolds flow measurements past a cylinder. A liquid filled prism can be used to correct for the radial distortions of SPIV for liquid flows. This method significantly improves the stereo-image focusing ability. The stereo method utilised here is able to provide high quality data of the flow past the cylinder.

Introduction

Standard 2D PIV allows one to measure two components of velocity with a single camera oriented orthogonally to the plane of measurement.In reality most flows are 3D in nature. Due to the physical nature of any experiment, even 2D flows experience some out-of-plane components. In these cases more information about the velocities in all 3 principal directions, u, v and w would be useful. The principles of stereoscopic imaging is well established and documented and is omitted here [1, 3].

The 3D PIV technique can be divided into measurement of the velocity fields in a three-dimensional domain (3D 3C) and measurement of the three velocity components in a two-dimensional domain (3C 2D). This paper will focus on the latter. There are two basic SPIV configurations. The translation method [2, 5], which is omitted here and the angular offset method. The Angular offset configuration shown in figure 1 uses two cameras with lens axis perpendicular to the imaging sensor. The problem is that the best plane of focus is parallel to the image plane, not in the plane of the laser sheet. In order to have the entire field in focus a sufficiently large depth of field is required. This can be achieved by decreasing the lens aperture, but this decreases the image intensity as defined in the depth of field equation 1,

$$\delta z = 4(1 + M^{-1})^2 f\#^2 \lambda, \qquad (1)$$

where M is the camera magnification, $f\#$ is the f-number, and λ is the wavelength of the illuminating laser. As a result an increase in laser intensity is required to adequately illuminate particles in the object plane. When the camera angle is increased the required depth of field increases as well. An optimal range of camera angle between $30°$ and $45°$ is found to minimise the error in the measured velocity components, e_T, defined in equation 2.

$$e_T = (e_x^2 + e_y^2 + e_z^2)^{1/2}, \qquad (2)$$

where each term in the expression represents the mean square difference between the measured and actual velocity for a particular component of velocity. In order to obtain particles in good focus over the entire image plane, the Scheimpflug condition must be satisfied [2, 5]. The Scheimpflug condition is satisfied when the object plane, image plane and lens principle plane intersect at a common point. This can be achieved by mounting the camera at an angle and rotating the lens with respect to the images sensor until all particles are in good focus. The combination of the Schiempflug condition, sufficient laser intensity and adequate depth of field provides good quality stereo data with an out-of-plane velocity component resolved to a high degree of accuracy [2].

The aim of this study is to increase the accuracy of the measured out-of-plane velocity component by optimising the SPIV methodology applicable to liquid flows. This is as much dependent on the ability to acquire good quality PIV images from each stereo camera as the ability to account for the physical limitations of the experimental setup through optical or mathematical methods. In liquid flows, specifically with large contained test sections the air-glass-liquid interfaces is a major source of radial distortions that affects negatively the ability for the correlation the PIV images from the stereo cameras. Utilising a liquid filled prism corrects this distortion [5].

When viewing in liquid flows the variable index of refractions further introduces radial distortions which transform circular particles into ellipses which are smeared. This results in distorted correlation peaks and erroneous measurement of the particle displacement from the image correlations. Furthermore, the magnification varies over the entire field. This variation can be accounted for in the mathematical mapping of the images from distorted to undistorted space, discussed in section , but the radial distortion remains. The radial distortion creates blurred images that affect the quality of the PIV images from each camera. Poor image quality at this level is further deteriorated during the reconstruction procedure resulting in very high out-of-plane velocity error [5].

The purpose of this paper is to report on validation of a stereoscopic technique applied at the Laboratory for Turbulence research in Aerospace & Combustion. The paper will focus on the experimental technique as well as report on the results from calibration and validation experiments. These experiments are used to optimise the experimental methodology by 'fine-tuning' the optical and mathematical algorithms used. Furthermore, as a test case, some flow measurements behind a 2D cylinder at high Reynolds number are presented.

Experimental Technique

Apparatus & method

The experiments are conducted in a water tunnel at the Laboratory for Turbulence Research for Aerospace & Combus-

tion. The perspex working section measures 500*mm* x 500*mm* x 1000*mm*. The turbulence intensity in the core region of the test section is less than 0.35% at the freestream velocity of 92mm/s. Figure 2 illustrates the experimental layout. For the test case, a 2D cylinder of diameter, $d = 25mm$ is suspended vertically above the test section as shown in figure 2. The cylinder is mounted to an oscillating rig that can be towed along the top of the test section on a railing system. The cylinder has a bow of 0.5*mm* over 500*mm* span due to machining.

CCD cameras are mounted vertically onto a 3-axis translation stage, below the test section. An angular- displacement stereo-configuration is utilized. The cameras are fitted with 55*mm* Micro Nikkor Nikon lenses. For SPIV acquisitions, the lens aperture is operated at $f\#11$. The Scheimpflug angle is $3°$. The cameras view a common region in the test section through two separate liquid filled prisms. $11\mu m$ Potter's hollow glass fibre beads are used to seed the water tunnel. The particles are illuminated by laser light from a dual-cavity New Wave Nd:Yag laser, delivering 32*mJ* at a wavelength of 532*nm*. Using appropriate collimating optics and mirrors, a 3*mm* thick horizontal light sheet is created in the midspan region of the cylinder as shown in figure 2).

Stereo Acquisition

The ability to accurately determine the particle displacements is dependent on how accurately one is able to map from distorted image space to undistorted object space. This is dependant on the calibration process. An in-situ calibration technique, similar to Solof *et al*[6] it utilised here as it does not rely on accurate knowledge of the geometry of the stereo-camera setup and is able to account for all distortions encountered during the actual experiment. Each camera acquires calibration images in multiple planes over a distance corresponding to the thickness of the laser sheet. Using a template-matching digital image correlation scheme, the exact locations of calibration markers in distorted image space are found.

The calibration data is used to calculate the mapping function, f, using a least squares approach. A vector-valued polynomial with cubic dependence on the in-plane components, x and y and quadratic dependence on the out-of plane component, z is used. This function is expected to adequately track any distortions one expects to encounter in PIV images and is discussed in greater detail in Solof *et al*[6].

Double exposed images are acquired in a single planes along the span of the cylinder (z-direction). Based on the variance in the measured velocity 1000 instantaneous images are acquired. The bias error in the measurements is 1% at 99% confidence level. The acquired image pairs are analyzed using a adaptive multi-grid cross-correlation algorithm from Soria [7]. From the stereo images, the three components of velocity u, v and w and the out of plane vorticity,(ω_z) is derived from the velocity gradients using a local Chi-Sq fit of 13 data points. From the instantaneous velocity fields, the mean velocity field is derived. The stereo reconstruction algorithm, StereoMagik$^©$, interpolates the displacement information from the two separate PIV images onto a user defined regular grid by applying the mapping function. A reverse mapping combines the two component image displacements to three components of fluid displacements. The experimental setup is discussed in detail in [4].

Solid Body translations

In order to validate the SPIV technique a method similar to Bjorkquist [2] is adopted in which a known displacement is measured using SPIV. A PIV test surface is translated by a fixed distance. The displacement is measured using the SPIV tech-

nique and the variation between the actual and measured values is calculated. 80 grit sandpaper is used as a test surface.

Discussion of Results

The results from translating the sandpaper 1*mm* in all principle directions is shown in table 1. The values shown represent the RMS of the difference between the measured and actual value. It can be seen that the worst case is when the test block is translated in the z direction. In this case the RMS error in the translated direction is up to 4 times as high as the measured y displacement.

RMS	σΔx	σΔy	σΔz
1mm X	0.056	0.005	0.101
1mm Y	0.01	0.064	0.088
1mm Z	0.053	0.023	0.193

Table 1: RMS [px] error from solid body translations of 1*mm*.

Table 2 indicates the RMS error in locating the calibration markers accurately from the distorted calibration images. These values translate directly into the mapping of particles from distorted to undistorted space. This quality is dependant on the method employed to identify local points in the field of view, The adopted template correlation scheme is the latest in several improvements.

ΔX^1	ΔY^1	ΔX^2	ΔY^2
0.102	0.080	0.209	0.106

Table 2: RMS [px] mapping error.

Table 3 indicates the RMS residual error from the final calculation of the fluid displacements. This quantity indicates how accurately the SPIV reconstruction algorithm is able to determine the displacements by recalculating the location of the particles in image space once the displacements are determined. The superscripts 1 and 2 indicate the X or Y location of a particle as seen in camera 1 and camera 2 respectively.

ΔX^1	ΔY^1	ΔX^2	ΔY^2
0.0008	0.0064	0.0006	0.0063

Table 3: RMS [px] residual error.

The largest residual error originates from the y-component of each camera yet the mapping error is greater for the x-component. In general, the values are small compared to 32*px*, the interrogation window size selected for the PIV analysis. If the perspective distortions are actually linear then the use of higher order polynomials as is the case here, would introduce error into the solutions for the fluid displacements. The largest RMS error obtained is 10 times larger than those obtained by Bjorkquist. [2]

Summary

The radial distortions associated with SPIV measurements in large volume liquid flows can be alleviated by using liquid-filled prisms. While the values obtained for both the mapping and residual errors are larger than those SPIV errors obtained by others, the errors are low. Furthermore, the validation experiments show that the technique and setup has been 'tuned' to measure and resolve the three components of velocity in a 2D plane to within 0.2px for the worst case. In the case of the measured test flow case at RE 15000, the mean profiles are similar
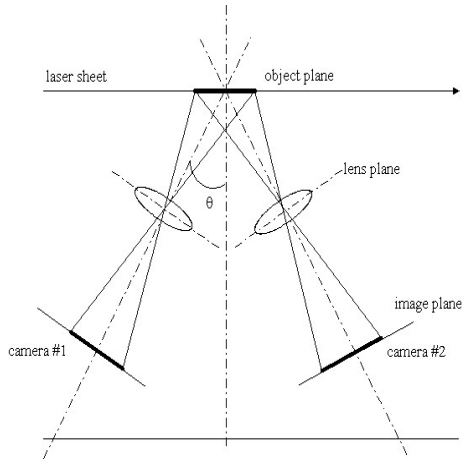
Figure 1: Stereo-camera angular offset configuration.

to other measured profiles for this flow regime. The RMS error is greatest in the core region of the wake but at overall low levels indicative of the quality of the measurement and methodology. Further refinement and adaptation of the SPIV technique is ongoing.

Acknowledgments

References

[1] Greated C. A. Arroyo M. P. Stereoscopic particle image velocimetry. *Meas. Sci. Technol.*, 2:1181–1186, 1991.

[2] Bjorkquist D. Design and calibration of a stereoscopic piv system. In 9th *International Symposium on Applied Laser Techniques to Fluid Mechanics*, Lisbon, Portugal, July 13-16 2001.

[3] Kompenhans J. Kahler C. J. Fundamentals of multiple plane stereo particle image velocimetry. *Exp. Fluids*, 30:70–77, 2000.

[4] Soria J. Parker K., von Ellenrieder K. D. The flow of a three-dimensional thrust producing wing. In Krogstad P. A. and Andersson H. I., editors, *Advances in Turbulence X. Proceedings of the 10th European Turbulence Conference*, volume 49 of *Fluid Mechanics and its Applications*, pages 11–14, Trondheim, Norway, June/July 2004. CIMNE.

[5] Jensen K. Prasad A, K. Scheimpflug stereocamera for particle image velocimetry in liquid flows. *Appl. Optics*, 34(30):7092–7099, 1995.

[6] Liu Z. C. Soloff S. M., Adrian R. J. Distortion compensation for generalized stereoscopic particle image velocimetry. *Meas. Sci. Technol.*, 8:1441–1454, 1997.

[7] J. Soria. Multigrid approach to cross-correlation digital PIV and HPIV analysis. In *Proceedings of 13th Australasian Fluid Mechanics Conference*. Monash University, 1998.
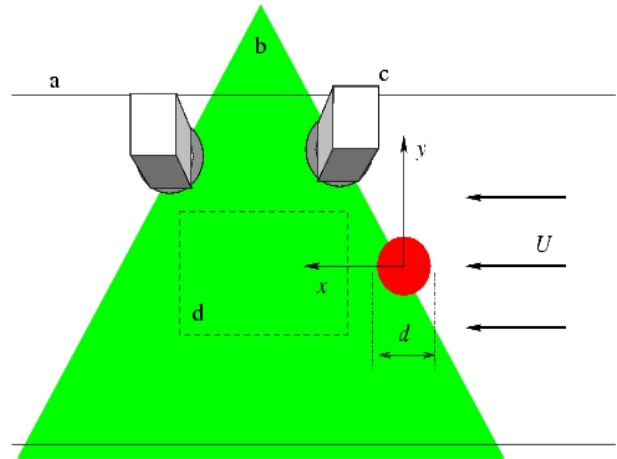
Figure 2: Schematic of the experimental apparatus: a) test section, b) laser sheet, c) stereo-CCD camera arrangement, d) imaged region of interest.
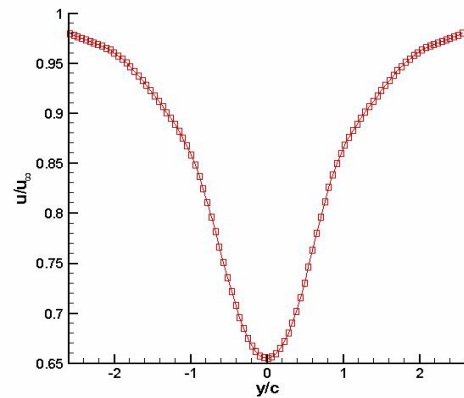

Figure 3: Mean velocity profile of u-component velocity behind a 25mm cylinder measured 6d from cylinder centre. Velocity is non-dimensionalised by the freestream velocity, u_∞.
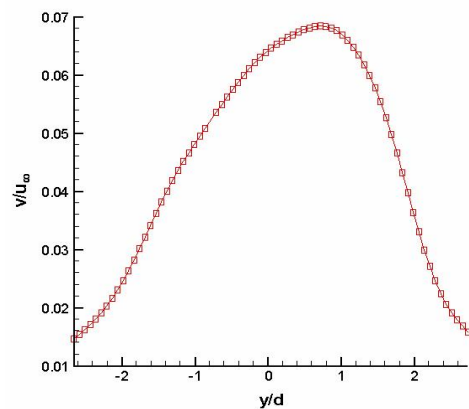

Figure 4: Mean velocity profile of v-component velocity behind a 25mm cylinder measured 6d from cylinder centre. Velocity is non-dimensionalised by the freestream velocity, u_∞.
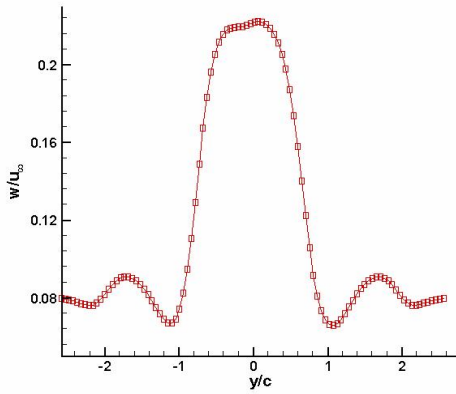
Figure 5: Mean velocity profile of w-component velocity behind a 25mm cylinder measured 6d from cylinder centre. Velocity is non-dimensionalised by the freestream velocity, u_∞.
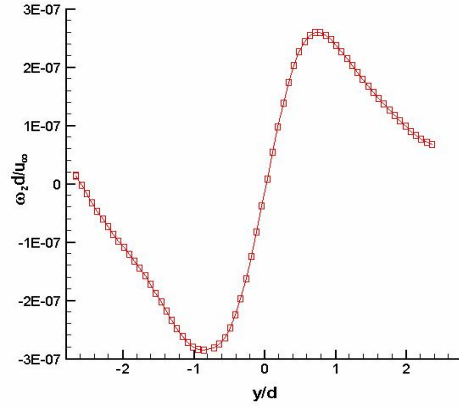

Figure 8: Mean out-of-plane vorticity profile behind a stationary cylinder of diameter 25mm measured 6d from cylinder centre. Vorticity is non-dimensionalised by the convective time scale, u_∞/d.
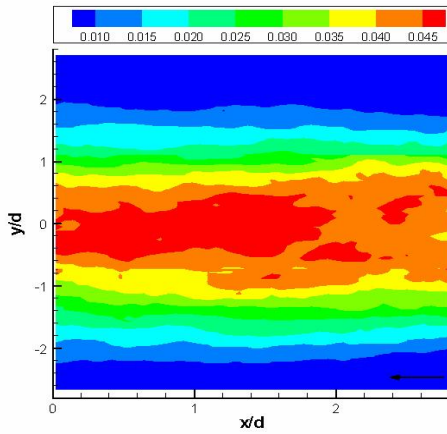

Figure 6: Iso-contour of the mean square error in u-component velocity, non-dimensionalised by the square of the freestream velocity, u_∞^2. Arrow indicates flow from right to left
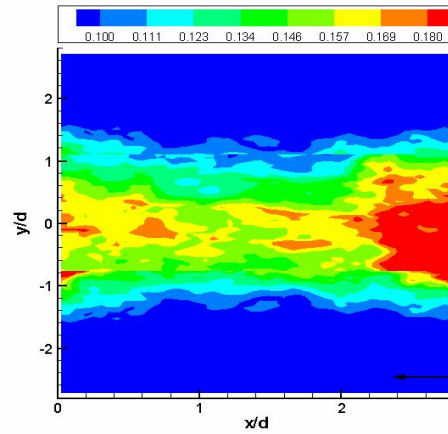

Figure 9: Iso-contour of the mean square error in w-component velocity, non-dimensionalised by the square of the freestream velocity, u_∞^2. Arrow indicates flow from right to left
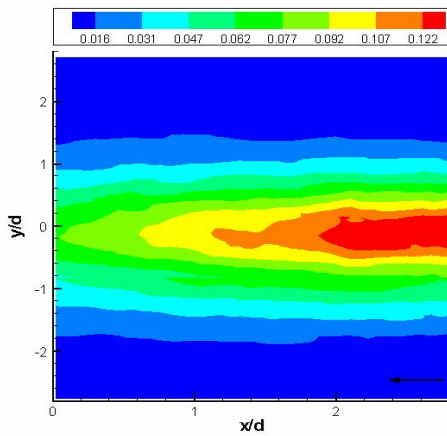

Figure 7: Iso-contour of the mean square error in v-component velocity, non-dimensionalised by the square of the freestream velocity, u_∞^2. Arrow indicates flow from right to left
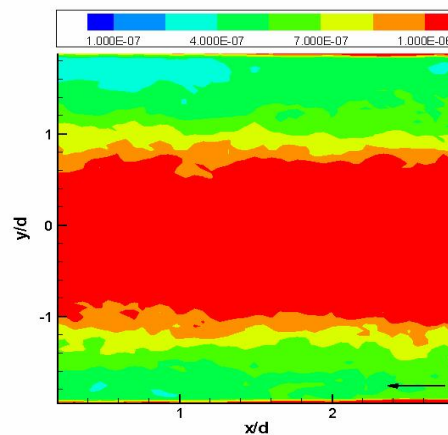

Figure 10: Iso-contour of the mean square error in out-of-plane vorticity components, ω_z, non-dimensionalised by the square of the convective timescale, $(u_\infty/d)^2$. Arrow indicates flow from right to left